PERGAMON

Available online at www.sciencedirect.com
SCIENCE DIRECT®

Acta Astronautica 56 (2005) 139–145

ACTA ASTRONAUTICA

www.elsevier.com/locate/actaastro

Aps-based miniature sun sensor for earth observation nanosatellites

Marcello Buonocore, Michele Grassi*, Giancarlo Rufino

Dipartimento di Scienza e Ingegneria dello Spazio, Università di Napoli "Federico II", P.le Tecchio 80, 80125 Napoli, Italy

Available online 19 October 2004

Abstract

This paper describes the research activity at the university of Naples concerning the design and prototype development of a low-cost APS-based miniature sun sensor for micro/nanosatellites applications. In the paper the sensor architecture is described, as well as the development of its prototype and of the facility for laboratory testing. Part of the project is also the development of a numerical code to simulate the sensor operation and predict the sensor performance. Numerical results show that an angular accuracy better than 1 arcmin is achievable.

1. Introduction

The miniature sun sensor is developed in the framework of a research project financed by the Italian Space Agency aimed at demonstrating some technological issues related to formation flying, such as autonomous guidance, navigation and control. Over the last few years one type of aerospace system architecture that has received increasing attention is one which has a distributed nature. Advanced concepts of aerospace platforms flying in formation have been studied and proposed for a variety of applications ranging from remote sensing to astronomy. Formation concept is widely considered as a unique tool to perform missions otherwise impossible. In addition, the formation concept offers several advantages in terms of increased survivability and reliability. NASA and US Air Force have identified multiple spacecraft formation flying as an enabling technology for future missions and a number of researchers are exploring the different aspects of formation flying. A number of space missions are under development which, in full or in part, make use of the formation concept: Earth Orbiter, Space Technology 3, Space Technology 5, Starlight by NASA; the American University Nanosatellites Program, which is based on several nanosatellites developed by several American Universities under private and public sponsorships; Cluster, Darwin, and Smart-2 by ESA; LISA jointly by NASA and ESA; TechSat21 by the Air Force Research Laboratory.

Technological feasibility of formation concepts relies also on the increasing reduction in space system mass, size and power requirements over the last few years. Thanks to the evolution of Micro Electro Mechanical System (MEMS) technology and micro-electronics, a number of scientific and technology demonstration missions based on the use of micro/nanosatellites have been flown by universities

* Corresponding author. Tel.: +39 081 7682217; fax: +39 081 7682160.
E-mail address: grassi@unina.it (M. Grassi).

0094-5765/$ - see front matter © 2004 Elsevier Ltd. All rights reserved.
doi:10.1016/j.actaastro.2004.09.006

and space agencies. Earth remote sensing missions have been proposed and carried out, and particular efforts are being made to fly high-resolution sensors on board micro-satellites. NASA and DOD are studying the use of micro-engineered systems in space. JPL is using this technology to develop "smaller, faster, cheaper" space systems for interplanetary missions. With NASA "New Millennium" and "X-2000" programs, coming years will see the development of many 10-kg spacecrafts equipped with micro-devices [1]. In 1997 the European Space Agency (ESA) identified micro/nanotechnologies as the critical technologies of future space programs [2]. Among the various issues, one concerning the development and integration of micro-accelerometers, micro-gyroscopes and high-performance CCD-based sensors for navigation was identified. Indeed, autonomous navigation is one of the most demanding requirements in modern space systems. Autonomy means collecting a number of flight information and, therefore, integrating a number of sensors on-board the vehicle. In this ambit, the use of micro-technologies is a promising solution. In this view, recently a number of studies have been performed to design miniature sensors. In particular, the availability of Active Pixel Sensor (APS) technology (in which detector and electronics are integrated on a single chip) has led to the development of advanced star sensor and sun sensors for attitude determination [3–5]. The replacement of CCDs with CMOS sensing devices in space applications is a topic under investigation [6,7]. CMOS technology has many advantages on CCD such as low-power consumption, single voltage supply needed (3.3 or 5 V), increased radiation hardness, simplified qualification procedures, capability of local reset and readout, on-chip integrated timing, control, and analog-to-digital conversion. Unfortunately, CMOS sensors noise performance is worse than CCDs [8,9].

In this framework, the research team at the University of Naples is developing the prototype of a miniature, low-cost, two-axis digital sun sensor. This is performed also thanks to the experience already gained by the research team in the development of a CCD-based star sensor prototype. This paper describes the sensor architecture, the sensor simulation code, the sensor prototype and laboratory test facility development. Numerical simulation results are shown which provide and estimate the sensor performances in terms of angular accuracy.

2. Sensor architecture and operation

The two-axis miniature sun sensor has a field of view of $\pm 60°$ and estimated final mass and power consumption of about 300 g and few mW, respectively. The sensor architecture basically consists of a radiation-hardened APS detector (STAR250, Fill-Factory^{TM}), which is an array of 512 × 512 25-μm active pixels, and of a mask with a number of equidistant tiny holes (with diameter of 0.2 mm in the prototype) placed on the top of the APS. The sun light passes through the mask and images of the sun are formed on the detector plane. Each image centroid is then evaluated, by an effective centroiding algorithm, allowing multiple measurements of the sun line direction to be performed. Fig. 1 shows a schematic of the mask layout and the centroiding concept for a single hole.

The image centroid coordinates, x_c and y_c, can be computed as the coordinates of the balance point of the image intensity function according to the following well-known expression [10]:

$$x_c = \frac{\int\int_{A_{wcn}} x I(x, y)\,dx\,dy}{\int\int_{A_{wcn}} I(x, y)\,dx\,dy},$$
$$y_c = \frac{\int\int_{A_{wcn}} y I(x, y)\,dx\,dy}{\int\int_{A_{wcn}} I(x, y)\,dx\,dy}, \quad (1)$$

where x and y are the geometric coordinates in the focal plane reference frame (X_{CA}, Y_{CA}, Z_{CA}), A_{wcn} is the area of the centroiding window (CW) containing the whole sun image, $I(x, y)$ is the image intensity function (i.e. the irradiance distribution on the focal plane). Nevertheless, it must be considered that the image provided by the sensor is discrete, since the image intensity function $I(x, y)$ is sampled at the pixel positions (each sample is proportional to the integral of the image irradiance on the pixel sensing area [11]). As a consequence, the centroid coordinates are given by summations extended to the n pixels of the CW as

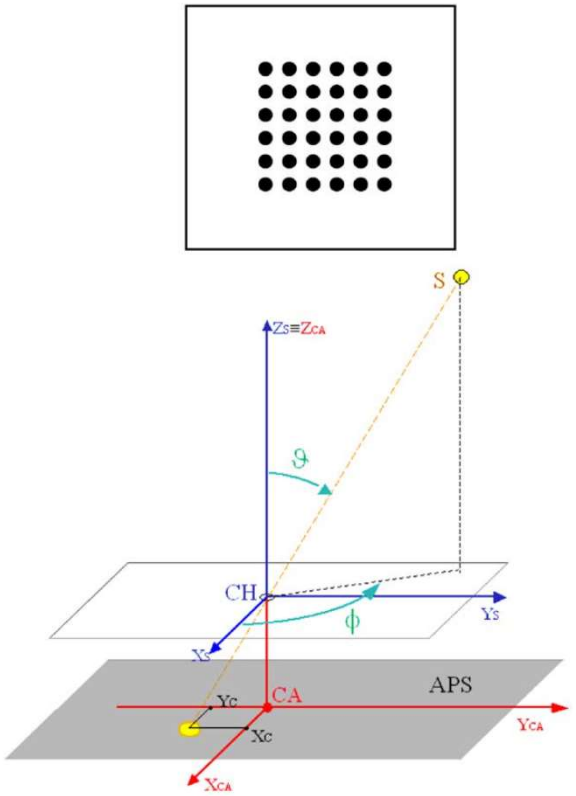

Fig. 1. Mask scheme and centroiding concept.

follows [10]:

$$\tilde{x}_c = \frac{\sum_{k=1}^{n} x_k I_k}{\sum_{k=1}^{n} I_k}, \quad \tilde{y}_c = \frac{\sum_{k=1}^{n} y_k I_k}{\sum_{k=1}^{n} I_k}, \tag{2}$$

where x_k and y_k are the coordinates of the kth pixel geometric centre and I_k is the image intensity function value detected at the same pixel. Concerning the identification of the CW, the procedure described in the following has been preliminarily identified. At the beginning of the centroiding procedure, the sun image on the focal plane must be identified, i.e. the illuminated pixels must be searched for. To this end, first of all the background level mean is evaluated using the pixels at the border of the APS. Then each pixel in the array is thresholded with the level selected at three times the background mean. Then, once a pixel above the selected threshold is detected, the CW is centred on the identified pixel and the centroiding algorithm is implemented. Concerning the CW size, two options have been preliminary considered: a CW of size about two times the sun image size (CW1), which can be used in a pre-processing phase, and a CW just containing the sun image (CW2), which can be used in a post-processing (or tracking) phase.

3. Sensor simulation and performance estimate

A simulation program has been developed to simulate the sensor operation and preliminary evaluation of sensor performance. The numerical code, running in MATLAB^{TM}, simulates each pixel response (in terms of number of produced photoelectrons) to the sun radiation by accurately modelling the sensor architecture, the APS spectral response and technical characteristics, the sun spectral emission and illumination geometry. In particular, the number of photoelectrons produced by each pixel has been evaluated according to [11]

$$n_{pe} = \frac{1}{q} A_S \frac{A_D}{H^2} \int_{\lambda_1}^{\lambda_2} \frac{M(\lambda)}{\pi} R(\lambda)\, d\lambda\, t_{INT}, \tag{3}$$

where q is the electron charge, A_S is the source area, A_D is the photodetector area, H is the distance of the photodetector by the source, $M(\lambda)$ is the spectral emittance of the sun (assumed as a black body at 6000 K), $R(\lambda)$ is the photodetector spectral response, and t_{INT} is the integration time. For the numerical implementation of Eq. (3) the illumination geometry of each pixel has been evaluated. In addition, in order to avoid pixel saturation, the integration time has been set at the minimum value (67 μs). This allows the pixel output to be kept within 80% of the photoresponse linearity range (with the solar flux attenuated 250 times by means of a filter). Fig. 2 shows a MATLAB^{TM} simulation of the sun image on the APS detector for a single-hole mask.

The image centroiding error has two contributions. The first one is a systematic error, coming from the use of Eq. (2) in which x_k and y_k are not the coordinates of the balance point of the irradiance distribution over the kth pixel. The second contribution arises from the fact that the detected I_k is affected by uncertainty, $\sigma_{I,k}$, due to various noise sources [11,12]. Therefore, assuming that the two errors are not correlated, the centroiding

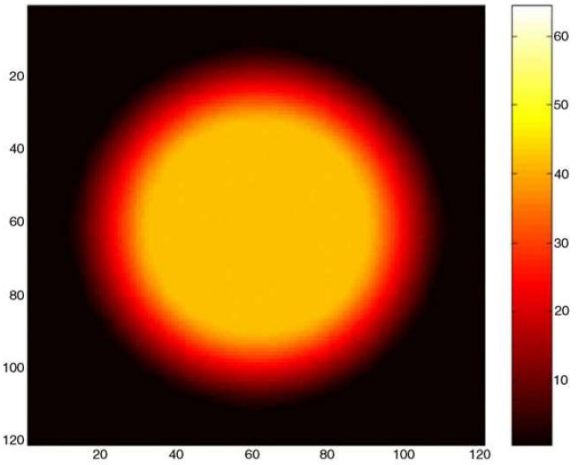

Fig. 2. Matlab simulation of the sun image.

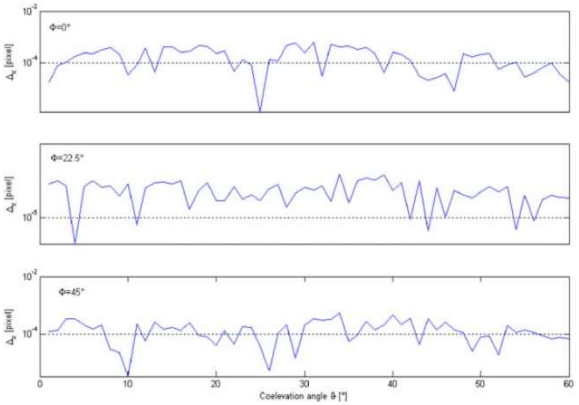

Fig. 3. Centroiding systematic error.

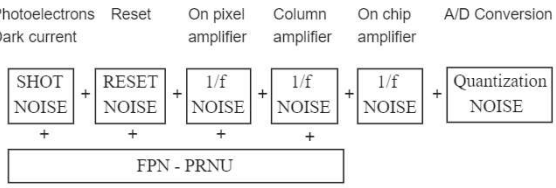

Fig. 4. APS noise model block diagram.

uncertainty is given by the following expression [13]:

$$\sigma^2_{\tilde{x}_c} = \sum_{k=1}^{n} \left[\left(\frac{\partial \tilde{x}_c}{\partial x_k} \right)^2 \sigma^2_{x,k} + \left(\frac{\partial \tilde{x}_c}{\partial I_k} \right)^2 \sigma^2_{I,k} \right], \tag{4}$$

where $\sigma_{x,k}$ is the error resulting from the use of pixel geometrical centres instead of the balance points of the irradiance distribution over single pixels. Taking the derivatives in (4) it finally results

$$\sigma^2_{\tilde{x}_c} = \sum_{k=1}^{n} \left[\left(\frac{I_k}{I_{tot}} \right)^2 \sigma^2_{x,k} \right] + \left(\frac{1}{I_{tot}} \right)^2 \times \sum_{k=1}^{n} [(x_k - \tilde{x}_c)^2 \sigma_{I,k}]. \tag{5}$$

Fig. 3 shows the systematic error in $\tilde{x}_c$ versus the sun coelevation angle for three values of the azimuth. The systematic error is of the order of 10^{-4} pixel. It has been numerically evaluated as the difference between the centroid and sun centre x-coordinates on the focal plane (a similar diagram is obtained for the y coordinate).

Fig. 4 shows the block diagram of the APS adopted noise model [10]. The rms contribution of the shot noise has been evaluated as $\langle n^2_{shot} \rangle = n_{phe} + n_{dark}$, where n_{dark} is the number of dark current electrons [11,14].

The rms contribution of the quantization noise can be evaluated as $\langle n^2_{quant} \rangle = n_{WELL}/2^N\sqrt{12}$, where n_{WELL} is the number of the full well electrons [11] and N is the number of bits of the sensor analog-to-digital converter. The $1/f$ noise of the amplifiers is removed by means of double-sampling techniques [11,12]. The other contributions can be evaluated with reference to the sensor data sheet [12]. The total number of noise electrons rms value $\langle n_{nope} \rangle$ is therefore given by the following expression:

$$\langle n_{nope} \rangle = [\langle n^2_{shot} \rangle + \langle n^2_{reset} \rangle + \langle n^2_{1/f} \rangle + \langle n^2_{FPN} \rangle + \langle n^2_{PRNU} \rangle + \langle n^2_{quant} \rangle]^{1/2}. \tag{6}$$

Table 1lists the main characteristics of the STAR 250^{TM} photodetector.

Fig. 5 shows the photodetector noise, evaluated at the image centre pixel, as a function of the coelevation angle (azimuth is zero). Fig. 6 shows the centroiding error due to the photodetector noise as a function of the sun coelevation angle for three representative values of the azimuth. As expected, the error increases with the coelevation angle due to the sun image elongation on the focal plane. The error increases with the CW size, as well. In particular, it can be seen that if CW1 is used the theoretical angular error is given by $0.04 \times$

Table 1
STAR250 characteristics

	Fillfactory^{TM} STAR 250^{TM}
Pixel array	512 × 512 pixels
Pixel size	25 × 25 μm^2
Full well capacity	311 Ke$^-$
Conversion gain	5.7 μV/e$^-$
Dark current	4750 e$^-$/s @ room temp.
Reset noise	76 e$^-$
FPN	1σ < 0.1% of full well
PRNU	1σ < 1.3% of signal

Table 2
IBIS4 Characteristics

	Fillfactory^{TM} IBIS4^{TM}
Pixel array	1280 × 1024 pixels
Pixel size	7 × 7 μm^2
Full well capacity	70 Ke$^-$
Conversion gain	18 μv/e$^-$
Dark current	1055 e$^-$/s @ room temp.
Temporal noise	20 e$^-$
FPN	1σ < 0.2% of full well
PRNU	1σ < 2.5% of signal

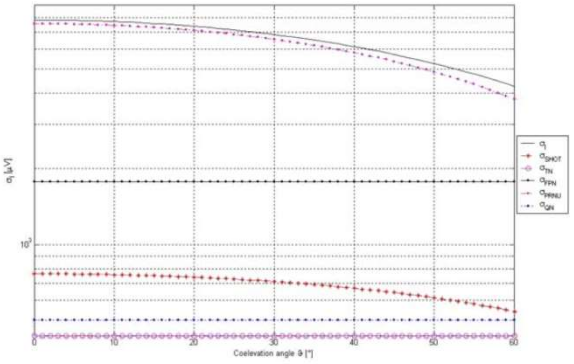

Fig. 5. STAR250 noise versus the coelevation angle (image centre pixel).

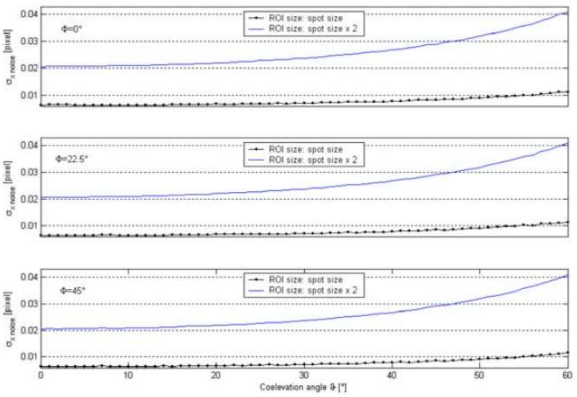

Fig. 6. Centroiding error due to noise versus the coelevation angle (one-hole mask).

0.48° = 0.019° (where 0.48°is the pixel IFOV), i.e. about 1 arcmin. If CW2 is used, the theoretical angular error reduces to about 17 arcsec.

4. Sensor prototype and test facility

In order to validate the sensor concept, a prototype of the sensor and a test facility have been developed at the University of Naples as part of the project. To limit costs, the sensor prototype adopts a low-cost APS detector, which is an array of 1280 × 1024–7 μm active pixels (Fill-Factory^{TM} IBIS4 demo-board, see Table 2 and Fig. 7). In order to perform measurements with an increasing number of holes several MEMS masks have been developed together with a mask holder/adapter to assemble the masks on the detector board. The 0.1-mcm thick steel mask prototype consists of equally spaced 0.2-mm diameter holes and it is placed at a distance of about 3 mm from the APS plane, allowing a field of view of about ±60° to be realized. The mask prototype has been manufactured with a low-cost process (electron discharge machining) which allows a precision of about 0.01 mm in the hole diameter manufacturing (Fig. 8).

The sun simulator consists of a 1000 W XENON ARC LAMP (ORIEL Instruments^{TM}), whose power output is driven to an integrating sphere (ORIEL Instruments^{TM}) by an optical fibre, and of a collimating lens. The APS demo-board with the mask holder is assembled on a precision rotating stage (PHYSIK INTRUMENTE^{TM}) in order to reproduce different sun aspect angles. The distance of the sensor prototype from the solar source is regulated by a micro-positioning system. The whole system is assembled on an optical table at the aerospace laboratory of the Second University of Naples. At the moment, only the sensor rotation along the axis perpendicular to the optical table can be performed. Fig. 7 collects photographs showing the system main

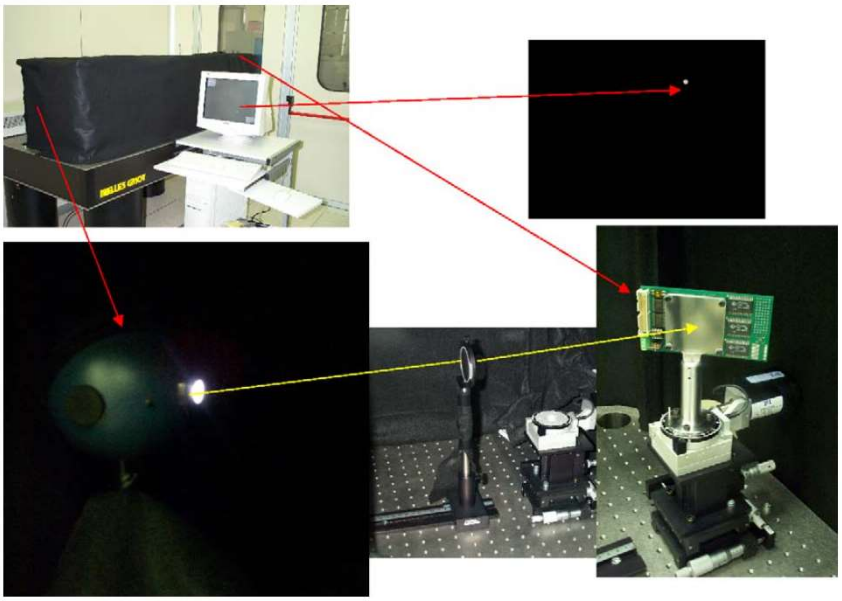

Fig. 7. Test system.

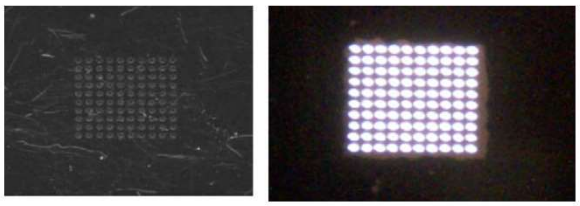

Fig. 8. Mask details.

components. The rotation of the rotating stage is performed by remotely controlling a stepper motor which allows incremental rotations of about 1 arcsec. For laboratory test results to be useful to predict the sensor performance, the prototype has been designed so that the same spot size is realized on the focal plane (i.e. the same focal length is realized). To this end, only one-half of the FOV has been implemented in the sensor prototype, by properly positioning the mask holes. Numerical simulations show that the prototype exhibits performances comparable to the ones of the STAR 250 sensor (Figs. 9 and 10).

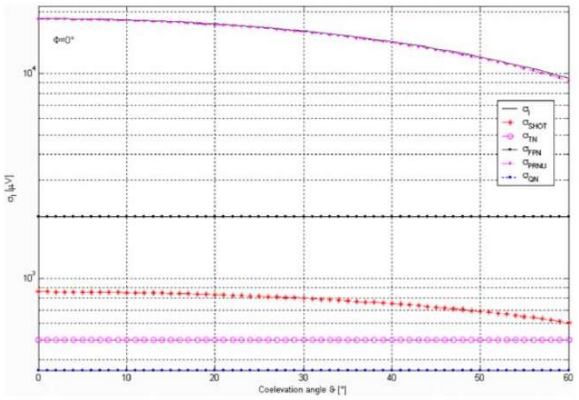

Fig. 9. IBIS4 noise versus the coelevation angle (image centre pixel).

Indeed, the angular error is about 0.017°(i.e. 1 arcmin), if the CW1 is selected, and reduces to about 0.006°(i.e. about 22 arcsec), if the CW2 is considered. This arises from the fact that the STAR250^{TM} and IBIS4^{TM} photodetectors have similar signal-to-noise ratios. As a consequence, the IBIS4^{TM} photodetector exhibits theoretical performances comparable with the STAR250^{TM} ones.

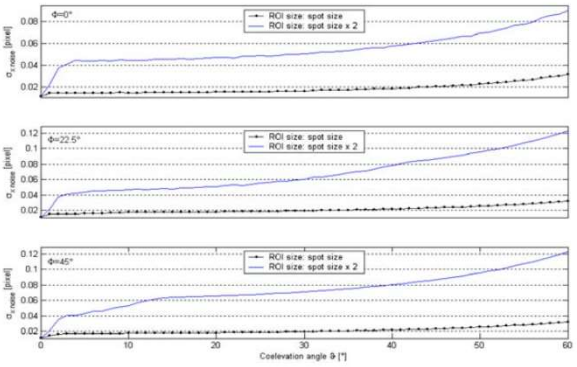

Fig. 10. Centroiding error due to noise versus the coelevation angle (one-hole mask).

5. Conclusions

The paper describes the work carried out at the University of Naples concerning the development of a miniature APS-based sun sensor for micro/nanosatellite attitude determination. The sensor is designed in order to minimize cost, mass and power consumption. To this end, the sensor architecture is based on a MEMS mask, consisting of one or more tiny holes, placed on the top of a CMOS photodetector. The sun-line direction is evaluated by determining the centroid of the sun image on the focal plane. A numerical code has been developed as part of the project to simulate the sensor operation and predict the sensor performances.

Numerical simulations show that with the implemented centroiding algorithm an angular accuracy better than 1 arcmin is achievable. A sensor prototype and a test system are being developed at the aerospace laboratory of the Second University of Naples to demonstrate the sensor concept and validate the numerical results. To reduce costs, commercial off-the-shelf components have been used to develop the sensor prototype. In particular, the APS is a commercial demoboard which integrates the photodetector and the electronics.

Acknowledgements

The work in the paper has been carried out with the financial contribution of the Italian Space Agency and the Ministry of University and Scientific Research.

References

[1] D. Collins, et al., Miniature, low cost, highly autonomous spacecraft—a focus on new millennium, IAF Paper 95-U.2.06 46th International Astronautical Congress, Oslo, Norway, 1995.
[2] Proceedings of the Second Round Table on Micro/Nanotechnology for Space, ESTEC, the Netherlands, 15–17 October 1997, ESA WPP-132.
[3] V.S. Kouzmin, et al., Miniature sun sensor, SPIE 2739 (1996) 407–410.
[4] J.H. Hales, M. Pedersen, Two-axis MOEMS Sun Sensor for Pico Satellites, 16th Annual AIAAA/USU Conference on Small Satellites, 2001.
[5] C.C. Liebe, et al., Micro sun sensor, IEEEAC paper #274, 2002.
[6] C.C. Liebe, L. Alkalai, G. Domingo, B. Hancock, D. Hunter, J. Mellstrom, I. Ruiz, C. Sepulveda, B. Pain, Micro APS based star tracker, Proceedings of the IEEE Aeroconference 5 (2002) 2285–2300.
[7] E. Fossum, et al., CMOS active pixel sensor star tracker with regional electronic shutter, IEEE Solid-State Circuits Journal 32 (2) (1997) 285–288.
[8] E.R. Fossum, CMOS image sensors: electronic camera-on-a-chip, IEEE Transactions on Electron. Devices 44 (10) (1997) 1689–1698.
[9] C.C. Liebe, Accuracy Performance of star trackers—a tutorial, IEEE Transactions on Aerospace and Electronic Systems 38 (2) (2002) 587–599.
[10] W.K. Pratt, Digital Image Processing, second ed., Wiley, New York, USA, 1991, pp. 636.
[11] G.C. Holst, CCD Arrays Cameras and Displays, second ed., SPIE Press, Washington WA, USA, 1998.
[12] Fill Factory, STAR 250 Datasheet, http://www.fillfactory.com, 2003.
[13] G. Rufino, D. Accardo, Enhancement of the centroiding algorithm for star tracker measure refinement, Acta Astronautica 52 (2) (2003) 135–147.
[14] H. Tian, B. Fowler, A. El Gamal, Analysis of temporal noise in APS, Proc. SPIE 3649 (1999) 177–185.